Desalination and Water Treatment
www.deswater.com

doi: 10.5004/dwt.2020.25816

193 (2020) 402–413
July

Polymeric composite materials based on silicate. III-Capacity and sorption behavior of some hazardous metals on irradiated doped polyacrylamide acrylonitrile

Mamadouh M. Abou-Mesalam, Mohamed R. Abass*, Asmaa B. Ibrahim, Essam S. Zakaria

Atomic Energy Authority, Hot Labs. Centre, Postal Code: 13759, Cairo, Egypt, Tel. +00201153334821; emails: mohamed.ragab@eaea.org.eg/ mohamed.ragab201400@yahoo.com (M.R. Abass), Tel. +00201112901869; email: mabumesalam@yahoo.com (M.M. Abou-Mesalam), Tel. +00201009327167; email: asmaabendary80@yahoo.com (A.B. Ibrahim), Tel. +00201003647990; email: essamzakareya@yahoo.com (E.S. Zakaria)

Received 30 August 2019; Accepted 6 March 2020

ABSTRACT

Chemically stable magneso-silicate (MgSi), polyacrylamide acrylonitrile P(AM-AN), and polyacrylamide acrylonitrile magneso-silicate [P(AM-AN)-MgSi] comparing with other ion exchangers ware synthesized at different radiation doses. The capacities of these composite materials for Ni^{2+}, Cd^{2+}, Co^{2+}, Pb^{2+}, Zn^{2+}, and Cu^{2+} were studied and the data revealed that the capacity of MgSi is higher that obtained P(AM-AN) by 0.6 value, and lower for [P(AM-AN)-MgSi] by 1.32 value. Distribution coefficients in HNO_3 show separation potentiality of prepared composites for studied cations and Cd^{2+} have higher separation factor to MgSi and P(AM-AN), while Pb^{2+} has higher separation factor to [P(AM-AN)-MgSi].

Keywords: Magneso-silicate; Radiation doses; Chemically stable; Capacity; Distribution coefficients

1. Introduction

The toxic heavy metals are very dangerous to health, for example, lead is considered as a highly toxic element when ingested or inhaled and adsorbed, it can harm virtually every system in the human body, especially kidney, brain, and reproductive systems of both male and females. Lead harms many body systems because it disrupts enzyme systems mediated by other metals important to the body such as iron, calcium, and zinc [1,2], so industrial wastewaters must be treated to remove the toxic metal ions before they can be discharged into the sewerage. Pb^{2+}, Cu^{2+}, Zn^{2+}, Cd^{2+}, and Ni^{2+} are common pollutants introduced into natural wastewaters from a variety of industrial wastewaters including those from the textile, electroplating, leather tanning, and metal finishing industries [2–4]. Accumulation of these hazardous ions in the environment caused great concern [4]. The removal of these metals from waters and wastewaters is important in terms of protection of public health and environment because heavy metals are non-degradable in the environment and can be harmful to a variety of living species [2,4,5]. Several techniques like adsorption, chemical reduction, photocatalytic, photodegradation process, and biological reduction have been used for the remediation of hazardous elements [5–8]. Ion exchange materials classified into organic, inorganic, and organic–inorganic hydride ion exchangers. Inorganic ion exchangers are superior to the organic resins with respect to thermal stability and resistance to radiation, they are highly selective for certain elements, as well as their chemical stability [9,10]. Organic ion exchangers are well-known for their uniformity, chemical stability, and control of their ion-exchange properties through synthetic methods [11]. To obtain a combination of these advantages associated with polymeric and inorganic materials as ion exchangers, attempts have been made to

* Corresponding author.

develop polymeric-inorganic composite ion exchangers by incorporation of organic monomers in the inorganic matrix, were found selective for heavy toxic metal ions and utilized for analysis of water pollution [2,5,9,12]. Many hybrid materials have been investigated for their chemical, biological, and environmental significance [9]. Synthetic ion exchangers are used for a wide range of different analytical application, such as environmental remediation [13,14], biochemistry [15], water softening [10], catalysis [10], hydrometallurgy [10], and selective adsorption [16,17] to medical applications [17–21]. Different inorganic ion exchange materials based on silicate and polyacrylamide acrylic acid silicon titanate were synthesized earlier by Abou-Mesalam et al. [10,15,22] and used for removal of some heavy metals from industrial and hazardous wastes.

In this work, chemically stable magneso-silicate (MgSi), polyacrylamide acrylonitrile P(AM-AN), and polyacrylamide acrylonitrile magneso-silicate [P(AM-AN)-MgSi] prepared at radiation doses 25, 65, and 90 kGy were investigated for ion exchange capacity, distribution coefficient, and separation factor for some toxic heavy metal ions.

2. Experimental

MgSi, P(AM-AN), and [P(AM-AN)-MgSi] materials were prepared as described earlier by Abou-Mesalam et al. [10,15,22].

2.1. Chemical stability

The chemical stability of MgSi, P(AM-AN), and [P(AM-AN)-MgSi] composites prepared at different radiation doses were carried out by mixing 100 mg of each sample and 100 mL of H_2O, (HNO_3 and HCl acid media) at different concentrations (10^{-3}–6 M) the desired solution with intermittent shaking for about 1 week at 25°C ± 1°C. The filtrate was tested gravimetrically [23].

2.2. Equilibrium time

All the measurements of equilibrium were carried out by shaking 0.2 g of MgSi, P(AM-AN), and [P(AM-AN)-MgSi] composites with 10 mL of Ni^{2+}, Cd^{2+}, Co^{2+}, Pb^{2+}, Zn^{2+}, and Cu^{2+} solutions in a shaker thermostat at 25°C ± 1°C with V/m = 50 mL/g. After each time interval, the shaker is stopped and the solution is separated at once from the solid. Then the filtrate was taken analyzed by atomic absorption spectrometer (AAS) for the determination of the concentration of the metal ions the percent uptake can be calculated by using the following equation [24]:

$$\%\,\text{uptake} = \left(\frac{C_i - C_f}{C_i}\right) \times 100 \tag{1}$$

where C_i and C_f the initial and final concentration of metal ions in solution, respectively.

2.3. Effect of batch factor (V/m)

Batch factor was optimized by shaking different weights of solids with different volume of studied cations (100 mg/L) to obtain varying V/m ratios (25, 50, 100, 200, and 400 mL/g). After an equilibrium, as the above equilibrium time experiment, the filtrate was taken analyzed for the determination of the concentration of the metal ions by AAS. The percent uptake can be calculated by using Eq. (1).

2.4. Capacity measurements

The capacities of MgSi, P(AM-AN), and [P(AM-AN)-MgSi] composites prepared at different radiation doses were determined by repeated equilibriums of the solids with Ni^{2+}, Cd^{2+}, Co^{2+}, Pb^{2+}, Zn^{2+}, and Cu^{2+} solutions. One gram of each solid material was equilibrated with 50 mL of 100 mg/L studied cation solutions by V/m = 50 mL/g. The mixture was shaken for 24 h at 25°C ± 1°C. After equilibrium, the filtrate was separated by centrifugation and replaced by the same volume of the initial solution. The procedure was repeated until no further absorption of cations occurred. The capacity was calculated from the following equation [17]:

$$\text{Capacity} = \text{uptake} \times C_i \times \frac{V}{m}\,\text{mg/g} \tag{2}$$

where C_i is the initial concentration of the solution, mg/L; V is the solution volume, mL; and m is the weight of the composite (g).

2.5. Effect of [H+] ion on distribution studies

Batch technique was followed to study the distribution coefficient (K_d) values on the different samples MgSi, P(AM-AN), and [P(AM-AN)-MgSi] composites prepared at different radiation doses as a function of different concentration of H^+ was studied using batch technique. 0.2 g of solids were shaken at 25°C ± 1°C with 10 mL of Ni^{2+}, Cd^{2+}, Co^{2+}, Pb^{2+}, Zn^{2+}, and Cu^{2+} solutions (100 mg/L) with a V/m ratio of 50 mL/g. The [H^+] concentrations were adjusted to (10^{-3}, 10^{-2}, 10^{-1}, 0.5, 1, 2, and 4). After an overnight standing the solution is separated at once from the solid and the filtrate was taken analyzed for the determination of the concentration of metal ions by (AAS). The distribution coefficient (K_d) and separation factor (α_B^A) values were calculated using the following equations [10,24]:

$$K_d = \left(\frac{C_i - C_f}{C_f}\right) \times \frac{V}{m}\,\text{mL/g} \tag{3}$$

$$\text{Separation factor}\left(\alpha_B^A\right) = \frac{K_d(B)}{K_d(A)} \tag{4}$$

where C_i and C_f the initial and final concentration of metal ions in solution, respectively, V is the solution volume (mL), and m is the composite mass (g), K_d (A) and K_d (B) are the distribution coefficients for the two competing species A and B in the system.

3. Results and discussion

The scope of this work is the attempt to study capacity and sorption investigation of a high chemical stable

inorganic, organic, and composite ion exchangers MgSi, P(AM-AN), and [P(AM-AN)-MgSi] composites.

The chemical stability of MgSi, P(AM-AN), and [P(AM-AN)-MgSi] composites prepared at different radiation doses were studied in H_2O, HNO_3, and HCl and the data are shown in Table 1. The data present indicated that all prepared samples are stable in studied media up to 6 M, and physically soluble in acid media greater than 6 M. The solubility values were increased with the increasing of the acid concentration. The chemical stability of MgSi in acid medium is agreed with the chemical stability of SiTi prepared by Abou-Mesalam [25]. Where P(AM-AN) and [P(AM-AN)-MgSi] composites are more stable than polyacrylonitrile titanium tungstophosphate prepared by El-Aryan et al. [26], especially at a high acid concentration (4 M HCl and HNO_3), and less stable than potassium hexacyanocobalt(II) ferrate(II)-polyacrylonitrile prepared by Nilchi et al. [27]. Also, the data reflect that MgSi has higher stability than P(AM-AN) and [P(AM-AN)-MgSi] composites, this may be due to the higher water content of polymer composites compared to MgSi, and also the higher crystallinity of MgSi than polymer composites as mention earlier in XRD studies [28]. Furthermore, the solubility decreased with the increase of radiation doses, this may be due to increasing of crosslinking in the polymers, where the crosslinking increases by increasing radiation dose. Moreover, the results found in Table 1, indicated that [P(AM-AN)-MgSi] composites have higher chemical stability than P(AM-AN) copolymers, this may be due to the higher crystallinity and complexation of [P(AM-AN)-MgSi] composites than P(AM-AN) copolymers.

The variation of percent uptake of Ni^{2+}, Cd^{2+}, Co^{2+}, Pb^{2+}, Zn^{2++}, and Cu^{2+} onto MgSi, P(AM-AN), and [P(AM-AN)-MgSi] composites with shaking time was carried out as shown in Fig. 1. Fig. 1 indicate that percent uptake increases with the increase in shaking time and maximum adsorption were observed at 24 h on all prepared composites. Therefore, we can consider these times are sufficient to attain equilibrium for studied cations onto prepared composites and used for all further experiments.

Optimization of the best batch factor (*V*/*m*) were carried out by study of the percent uptake of studied cation solutions (100 mg/L) on MgSi, P(AM-AN), and [P(AM-AN)-MgSi] ion exchangers. This has been done by shaking 10 mL of studied cations (100 mg/L) for 24 h with various amounts (0.025, 0.05, 0.1, 0.2, and 0.4 g) of solids. The ratios of *V*/*m* were 25, 50, 100, 200, and 400. The results are given in Fig. 2, from this figure, the percent uptake of investigated cations on the prepared composites decreases with increasing the (*V*/*m*) ratio and the ratio (25), is the best ratio for maximum retention value.

The ion exchange capacities of prepared composites for Ni^{2+}, Cd^{2+}, Co^{2+}, Pb^{2+}, Zn^{2+}, and/or Cu^{2+} were determined at 25°C ± 1°C. The data are tabulated in Table 2. Table 2 indicates that the affinity sequence for all cations is: $Cu^{2+} > Ni^{2+} \approx Co^{2+} > Pb^{2+} \geq Zn^{2+} > Cd^{2+}$ for MgSi, this sequence is in accordance with the unhydrated radii of the exchanging ions. The absorption of ions increases by the ease of entry ions with smaller unhydrated radii in the pores of the exchanger [10,23,29]. The high capacity of MgSi for Cu^{2+} may be due to the higher complexing ability of Cu^{2+} with the presence in

Table 1
Chemical stability of MgSi, P(AM-AN), and [P(AM-AN)-MgSi] prepared at different radiation doses in different media at 25°C ± 1°C

Sample	Radiation dose, kGy	Solubility (g/L at 25°C ± 1°C)												
		H_2O	HNO_3, M						HCl, M					
			10^{-3}	10^{-2}	10^{-1}	0.5	1	3	6	10^{-3}	10^{-2}	10^{-1}	0.5	1	3	6
MgSi	–	Below detection limit	0.0032	0.061	0. 12	0.21	0.29	0.32	0.65	0.0022	0.059	0.11	0.22	0.32	0.45	0.66
P(AM-AN)	25		0.0065	0.092	0.26	0.39	0.49	0.53	0.75	0.0049	0.073	0.21	0.29	0.52	0.62	0.78
	65		0.0061	0.085	0.25	0.35	0.44	0.5	0.71	0.0046	0.071	0.18	0.28	0.45	0.59	0.76
	90		0.0045	0.066	0.19	0.31	0.41	0.45	0.68	0.0042	0.069	0.15	0.26	0.41	0.55	0.74
[P(AM-AN)-MgSi]	25		0.0044	0.077	0.29	0.33	0.46	0.51	0.69	0.0045	0.071	0.16	0.29	0.38	0.49	0.71
	65		0.0038	0.072	0.26	0.31	0.41	0.42	0.67	0.0042	0.069	0.14	0.25	0.36	0.48	0.69
	90		0.0034	0.069	0.22	0.28	0.36	0.39	0.66	0.0036	0.062	0.12	0.24	0.32	0.47	0.68

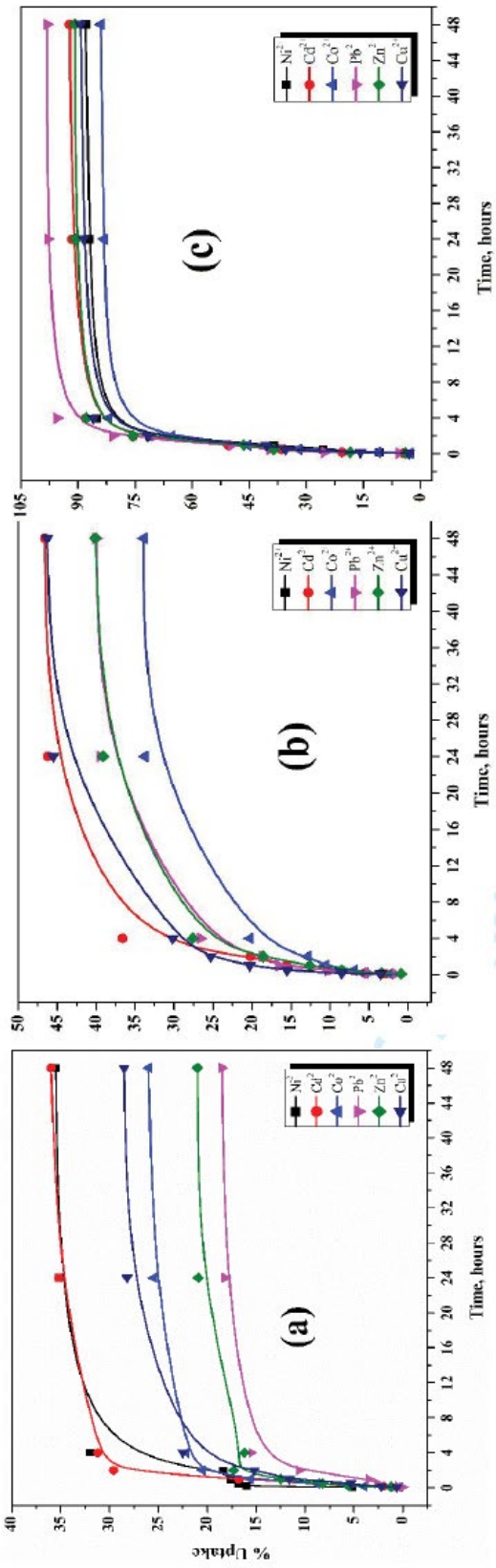

Fig. 1. Effect of contact time on % uptake of Ni^{2+}, Cd^{2+}, Co^{2+}, Pb^{2+}, Zn^{2+}, and Cu^{2+} on (a) MgSi, (b) P(AM-AN), and (c) [P(AM-AN)-MgSi] at 25°C ± 1°C.

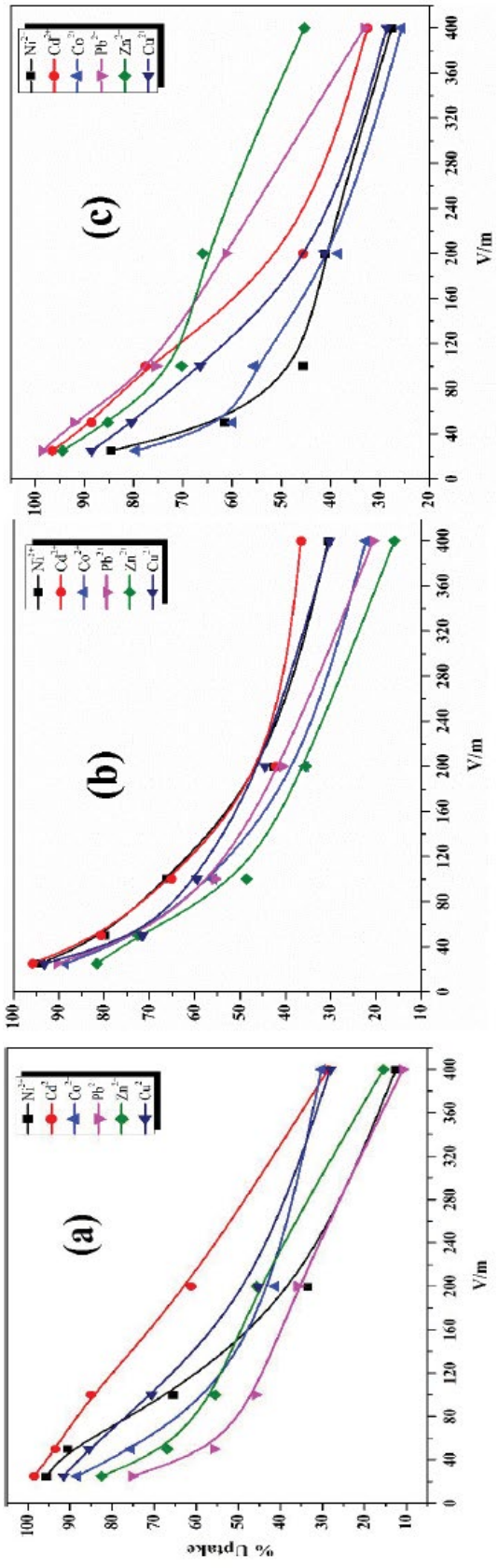

Fig. 2. Effect of *V*/*m* on % uptake of Ni^{2+}, Cd^{2+}, Co^{2+}, Pb^{2+}, Zn^{2+}, and Cu^{2+} on (a) MgSi, (b) P(AM-AN), and (c) [P(AM-AN)-MgSi] at 25°C ± 1°C.

Table 2
Capacity values of various exchanging ions onto MgSi, P(AM-AN), and [P(AM-AN)-MgSi] prepared at different radiation doses at 25°C ± 1°C

Exchanging ions	Ionic radii (Å)	Hydration energy	MgSi	
			Capacity, mg/g	Metal exchanging, as
Ni^{2+}	0.72	2,054	12.1	Unhydrated
Cd^{2+}	0.97	1,806	1.35	Unhydrated
Co^{2+}	0.72	2,054	12.0	Unhydrated
Pb^{2+}	1.20	1,480	4.8	Unhydrated
Zn^{2+}	0.74	2,044	4.5	Hydrated
Cu^{2+}	0.72	2,100	15.2	Unhydrated

Exchanging ions	Ionic radii (Å)	Hydration energy	P(AM-AN) at dose 25 kGy		P(AM-AN) at dose 65 kGy		P(AM-AN) at dose 90 kGy	
			Capacity, mg/g	Metal exchanging, as	Capacity, mg/g	Metal exchanging, as	Capacity mg/g	Metal exchanging as
Ni^{2+}	0.72	2,054	11.2	Unhydrated	11.3	Unhydrated	11.4	Unhydrated
Cd^{2+}	0.97	1,806	0.8	Unhydrated	1.5	Unhydrated	1.8	Unhydrated
Co^{2+}	0.72	2,054	12.2	Unhydrated	11.8	Unhydrated	11.9	Unhydrated
Pb^{2+}	1.20	1,480	2.2	Unhydrated	2.5	Unhydrated	4.8	Unhydrated
Zn^{2+}	0.74	2,044	3.44	Hydrated	4.2	Hydrated	5.3	Hydrated
Cu^{2+}	0.72	2,100	0.2	Hydrated	0.3	Hydrated	4.4	Hydrated

Exchanging ions	Ionic radii (Å)	Hydration energy	[P(AM-AN)-MgSi] at dose 25 kGy		[P(AM-AN)-MgSi] at dose 65 kGy		[P(AM-AN)-MgSi] at dose 90 kGy	
			Capacity, mg/g	Metal exchanging as	Capacity, mg/g	Metal exchanging, as	Capacity, mg/g	Metal exchanging, as
Ni^{2+}	0.72	2,054	12.6	Unhydrated	12.3	Unhydrated	11.8	Unhydrated
Cd^{2+}	0.97	1,806	3.2	Unhydrated	2.2	Unhydrated	1.9	Unhydrated
Co^{2+}	0.72	2,054	13.5	Unhydrated	13.0	Unhydrated	12.6	Unhydrated
Pb^{2+}	1.20	1,480	5.4	Unhydrated	5.4	Unhydrated	5.3	Unhydrated
Zn^{2+}	0.74	2,044	12.6	Unhydrated	10.6	Unhydrated	9.4	Unhydrated
Cu^{2+}	0.72	2,100	21.2	Unhydrated	23.2	Unhydrated	22.2	Unhydrated

more than one oxidation state. The lower capacity of MgSi for Cd^{2+} reflects the non-selectivity of MgSi for Cd^{2+}.

The data in Table 2 show that the capacity of P(AM-AN) composites prepared at different doses for studied cations are lower that obtained for MgSi by 0.6 value, with the sequence order for all cations is $Co^{2+} \geq Ni^{2+} > Zn^{2+} > Pb^{2+} > Cd^{2+} > Cu^{2+}$ for P(AM-AN) copolymers at 25 and 65 kGy. Whereas at 90 kGy P(AM-AN) copolymer has affinity sequence: $Co^{2+} \geq Ni^{2+} > Zn^{2+} \geq Pb^{2+} \geq Cu^{2+} > Cd^{2+}$ this sequence is supported that the unhydrated radii of the exchanging ions [29]. Also, the high capacity of P(AM-AN) for Co^{2+} may be due to the higher complexing ability of Co^{2+} with the presence in more than one oxidation states [10]. The lower capacity of P(AM-AN) for Cd^{2+} and Cu^{2+} reflects the non-selectivity of P(AM-AN) for these ions.

Also, the data in Table 2 reveal to the significant improvement in the capacity of [P(AM-AN)-MgSi] composites prepared at different doses for mentioned cations and become greater than obtained for MgSi by 1.32 value with the sequence order for all cations is $Cu^{2+} > Co^{2+} \geq Ni^{2+} \geq Zn^{2+} > Pb^{2+} > Cd^{2+}$. This sequence is supported that the unhydrated radii of the exchanging ions. The ions with smaller unhydrated radii easily enter the cavity of the exchanger, resulting in higher adsorption [10,29]. Also, a high capacity of [P(AM-AN)-MgSi] for Cu^{2+} may be due to the higher complexing ability of Cu^{2+} with the presence in more than one oxidation state. The lower capacity of [P(AM-AN)-MgSi] for Pb^{2+} reflects the non-selectivity of [P(AM-AN)-MgSi] for this ion. Also, the data in Table 2 shows a relatively high capacity of [P(AM-AN)-MgSi] compared to P(AM-AN) for the studied cations that, maybe due to the impregnation of MgSi to P(AM-AN) materials increases the number of acidic sites on the surface of [P(AM-AN)-MgSi] and hence increase the capacity [17].

Comparing these results with capacities of other materials, the capacities of prepared materials are greater than obtained for MgSi for Ni^{2+}, Co^{2+}, and Cd^{2+} removal [10] and MgSi, (Pam-Aa), and (Pam-Aa-MgSi) for Ni^{2+}, Cd^{2+}, Co^{2+}, Pb^{2+}, Zn^{2+}, and Cu^{2+} [23] and lower than the capacities of Fe_2O_3, Co-Fe_2O_3, and Ni-Fe_2O_3 for Pb(II) removal [30] and the adsorption capacities of T-NTO nanofibers for Pb(II) removal [31].

For studding selectivity of the ion exchange materials for metal ions for the separation of metal ions from the water system [9]. The distribution coefficients (K_d, mL/g) and separation factors (α) of investigated cations onto prepared composites in the range 10^{-3}–4 M HNO_3 medium are calculated and tabulated in Tables 3–5 and shown in Fig. 3. The preliminary studies indicate that the time of equilibrium for mentioned cations onto prepared ion exchangers was attained after 24 h in a shaker thermostat adjusted at 25°C ± 1°C.

The data in Tables 3–5 shows the inverse proportional was observed for the removal percentage with the $[H^+]$. The ion mobility of the mentioned cations is decreased by increasing $[H^+]$. The decrease of the ion mobility may be explained by an increase of the frictional forces exerted on the ions due to the change of the nature of hydrogen bonds in water [10,32,33]. As the proton concentration increases, the following water structure hydronium ions are formed H_3O^+, $H_5O_2^+$, $H_7O_3^+$, $H_9O_4^+$ modifying the structure of water, and thus the ion-water interaction. Also, the sorbent takes up the H^+ from the solution, hence, the surface becomes positively charged, which eventually restricts the uptake of investigated cations [32].

The data in Fig. 3 show that K_d values are inversely proportional to the $[H^+]$ of the media. By increase of the $[H^+]$ of the medium, the chance of the replacement of metal ions (Ni^{2+}, Cd^{2+}, Co^{2+}, Pb^{2+}, Zn^{2+}, and/or Cu^{2+}) with H^+ in the composite decreased that lead to a decrease of % uptake of these cations onto the composites.

Fig. 3a and Table 3 show the $[H^+]$ dependency of K_d values of studied cations onto MgSi. Linear relations between $\log K_d$ and $[H^+]$ were observed for Ni^{2+}, Cd^{2+}, Co^{2+}, Pb^{2+}, Zn^{2+}, and Cu^{2+} with slopes (0.28, 0.31, 0.25, 0.32, 0.37, and 0.13), respectively. These slopes did not equal to the valence of the metal ions sorbed, which prove the non-ideality of the exchange reaction. The variation may be due to the prominence of more than adsorption mechanisms other than ion exchange, like precipitation, surface adsorption, or simultaneous adsorption of anions [11,23,34].

The data in Table 3 indicate that K_d has the affinity sequence: $Cd^{2+} > Ni^{2+} > Cu^{2+} \approx Co^{2+} \geq Zn^{2+} \geq Pb^{2+}$ for MgSi, this sequence supported that the sorption of metal ions was carried out in unhydrated ionic radii except Cd^{2+} adsorbed as hydrated ionic radii [34,35], separation factor for the studied cations were calculated and indicated that, Cd^{2+} has a higher separation factor (2.6, 2.1, 2.0, 1.9, and 1.4) for Pb^{2+}, Zn^{2+}, Co^{2+}, Cu^{2+}, and Ni^{2+}, respectively, these values indicated that Cd^{2+} can easily separate from radioactive and industrial waste solutions included the above-mentioned cations, and these values reflect that non-selectivity of MgSi for Pb^{2+} [9].

The $[H^+]$ dependency of K_d values of studied cations onto P(AM-AN) at different radiation doses are shown in Figs. 3b–d and Table 4. Linear relations between $\log K_d$ and $[H^+]$ were observed for Ni^{2+}, Cd^{2+}, Co^{2+}, Pb^{2+}, Zn^{2+}, and Cu^{2+} with slopes [(0.35, 0.32, 0.28, 0.38, 0.37, and 0.27)], [(0.15, 0.32, 0.24, 0.4, 0.35, and 0.22)], and [(0.1, 0.33, 0.18, 0.32, 0.34, and 0.32)] for P(AM-AN) at doses 25, 65, and 90 kGy, respectively. These slopes are not equal to the valence of the adsorbed metals thus indicating a deviation from ideal ion exchange reactions. This variation may be determined by the prominence of a mechanism other than ion-exchange reactions [10,36]. It was found that the values of the distribution coefficient decrease with increasing $[H^+]$ values, which is a characteristic behavior of cationic exchanger [26].

From Table 4, it was found that the selectivity order of the investigated cations absorbed on P(AM-AN) at 25 kGy is $Cd^{2+} > Ni^{2+} > Cu^{2+} \geq Co^{2+} > Pb^{2+} \approx Zn^{2+}$ while the selectivity order at 65 kGy is $Cd^{2+} > Ni^{2+} > Cu^{2+} > Pb^{2+} > Co^{2+} > Zn^{2+}$ and the selectivity order at 90 kGy is $Cd^{2+} > Ni^{2+} > Cu^{2+} \geq Co^{2+} > Zn^{2+} > Pb^{2+}$. This sequence order supports the sorption of metal ions as unhydrated state except Cd^{2+} adsorbed as hydrated state, which may be due to the ionic radii. The ions with smaller ionic radii are easily exchanged and moved faster than that of ions with large ionic radii [36,37]. The separation factors for the studied cations on P(AM-AN) at different radiation doses were calculated and indicated that Cd^{2+} has a higher separation factor by (3.6, 3.4, 2.6, 2.5, and 1.3) for Zn^{2+}, Pb^{2+}, Co^{2+}, Cu^{2+}, and Ni^{2+} respectively, at 25 kGy. While Cd^{2+} has a higher separation factor by (4.9, 3.5, 3, 2.3, and 1.5) for Zn^{2+}, Co^{2+}, Pb^{2+}, Cu^{2+}, and Ni^{2+}, respectively, at

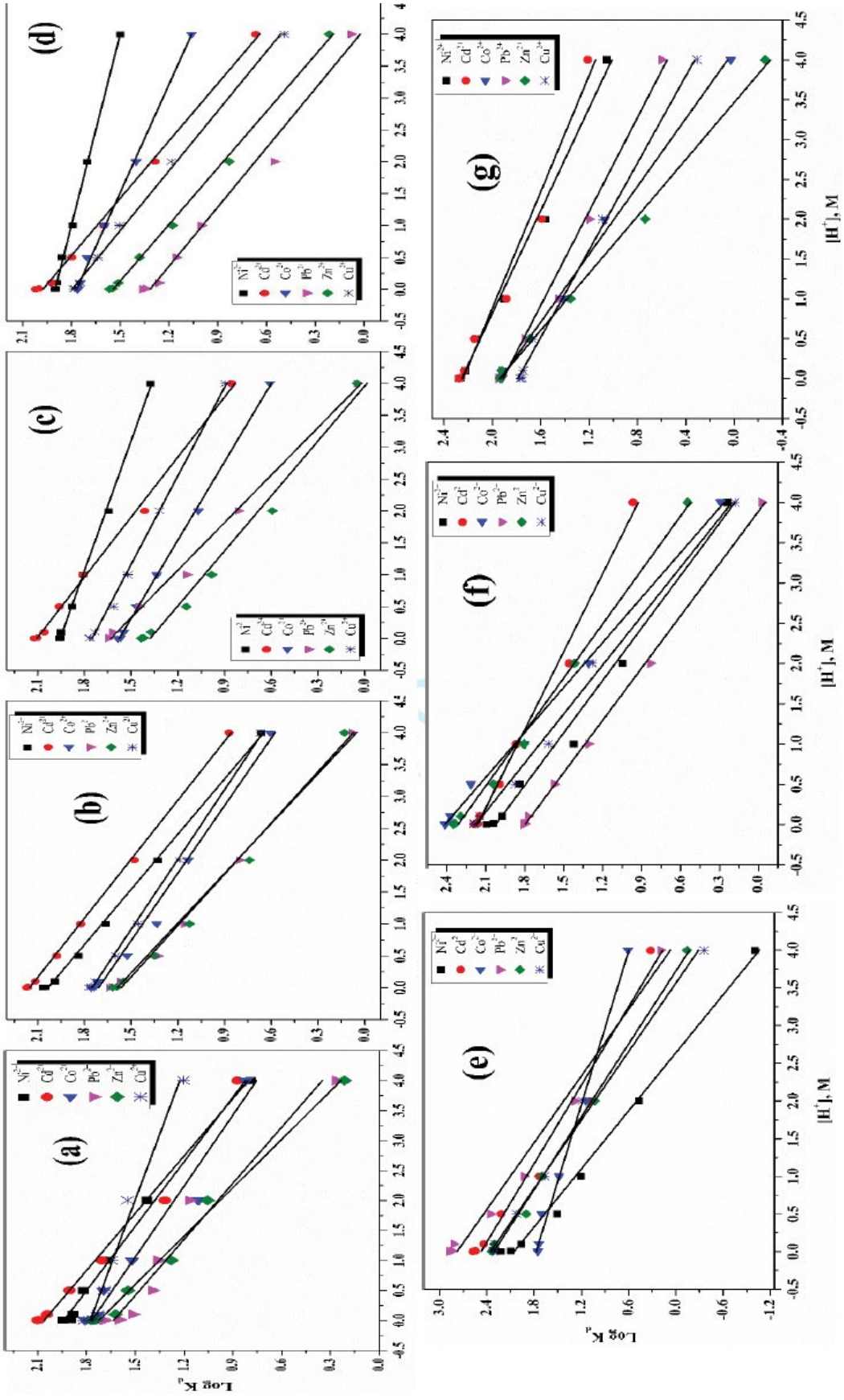

Fig. 3. Plots of logK_d against [H$^+$] of Ni^{2+}, Cd^{2+}, Co^{2+}, Pb^{2+}, Zn^{2+}, and Cu^{2+} onto (a) MgSi, (b–d) P(AM-AN) at dose 25, 65, and 90 kGy, respectively, and (e–g) [P(AM-AN)-MgSi] at dose 25, 65, and 90 kGy, respectively, at 25°C ± 1°C.

Table 3
K_d values and separation factors (α) for Ni^{2+}, Cd^{2+}, Co^{2+}, Pb^{2+}, Zn^{2+}, and/or Cu^{2+} onto MgSi at 25°C ± 1°C

[H^+]	K_d mL/g and (α)	Pb^{2+}	Zn^{2+}	Co^{2+}	Cu^{2+}	Ni^{2+}	Cd^{2+}
10^{-3}	K_d	49.1	59.2	64.6	65.3	88.6	126
	(α)		1.21	1.32	1.33	1.8	2.57
				1.09	1.1	1.5	2.13
					1.01	1.37	1.95
						1.36	1.93
							1.42
10^{-2}	K_d	39.9	55.2	57	57.1	78.9	123
	(α)		1.38	1.43	1.43	1.98	3.08
				1.03	1.03	1.43	2.23
					1	1.38	2.16
						1.38	2.15
							1.56
10^{-1}	K_d	32.8	41.8	53.9	53.7	76.4	110
	(α)		1.27	1.64	1.64	2.33	3.35
				1.29	1.28	1.83	2.63
					1	1.42	2.04
						1.42	2.04
							1.44
0.5	K_d	24.9	35.1	49.7	49.1	65.9	80.5
	(α)		1.41	2	1.97	2.65	3.23
				1.42	1.4	1.88	2.29
					0.99	1.33	1.62
						1.34	1.64
							1.22
1	K_d	22.9	19	33.1	44.4	48.1	51
	(α)		0.83	1.45	1.94	2.1	2.23
				1.74	2.34	2.53	2.68
					1.34	1.45	1.54
						1.08	1.15
							1.06
2	K_d	14.7	11.4	12.9	35.3	26.8	20.8
	(α)		0.78	0.88	2.4	1.82	1.41
				1.13	3.1	2.35	1.82
					2.74	2.08	1.61
						0.76	0.59
							0.78
4	K_d	1.8	1.6	6.6	16	6.2	7.4
	(α)		0.89	3.67	8.89	3.44	4.11
				4.13	10	3.88	4.63
					2.42	0.94	1.12
						0.39	0.46
							1.19

Table 4
K_d values and separation factors (α) for Ni^{2+}, Cd^{2+}, Co^{2+}, Pb^{2+}, Zn^{2+}, and/or Cu^{2+} onto P(AM-AN) at different radiation dose at 25°C ± 1°C

[H^+]	K_d mL/g and (α)	P(AM-AN) at dose 25 kGy						P(AM-AN) at dose 65 kGy						P(AM-AN) at dose 90 kGy					
		Zn^{2+}	Pb^{2+}	Co^{2+}	Cu^{2+}	Ni^{2+}	Cd^{2+}	Zn^{2+}	Co^{2+}	Pb^{2+}	Cu^{2+}	Ni^{2+}	Cd^{2+}	Pb^{2+}	Zn^{2+}	Co^{2+}	Cu^{2+}	Ni^{2+}	Cd^{2+}
10^{-3}	K_d		43.4	57	58.9	116	148	27.2	38.5	44.2	58.7	91.3	132	22.9	36.8	58.1	61.2	80	104
	(α)		1.04	1.37	1.42	2.79	3.56		1.42	1.63	2.16	3.36	4.88		1.61	2.54	2.67	3.49	4.54
		41.6		1.31	1.36	2.67	3.41			1.15	1.52	2.37	3.45			1.58	1.66	2.17	2.83
					1.03	2.04	2.6				1.33	2.07	3				1.05	1.38	1.79
						1.97	2.51					1.56	2.26					1.31	1.7
							1.28						1.45						1.3
10^{-2}	K_d		42	54.6	56.5	112	145	26.3	36.9	43.7	57.9	89.5	127	21.9	35.3	57.3	59.9	78.9	100
	(α)		1.08	1.4	1.45	2.87	3.72		1.4	1.66	2.2	3.4	4.83		1.61	2.62	2.74	3.6	4.57
		39		1.3	1.35	2.67	3.45			1.18	1.57	2.43	3.44			1.62	1.7	2.24	2.83
					1.03	2.05	2.66				1.32	2.05	2.91				1.05	1.38	1.75
						1.98	2.57					1.55	2.19					1.32	1.67
							1.29						1.42						1.27
10^{-1}	K_d		37	51.7	54.3	97.8	130	23.4	35.3	41.3	53.9	89.1	114	18.3	32.6	55.6	55.9	77.4	83.9
	(α)		1.04	1.46	1.53	2.75	3.66		1.51	1.76	2.3	3.81	4.87		1.78	3.04	3.05	4.23	4.58
		35.5		1.4	1.47	2.64	3.51			1.17	1.53	2.52	3.23			1.71	1.71	2.37	2.57
					1.05	1.89	2.51				1.31	2.16	2.76				1.01	1.39	1.51
						1.8	2.39					1.65	2.12					1.38	1.5
							1.33						1.28						1.08
0.5	K_d		21.3	33.5	39.8	69.2	95.1	13.9	29.1	28.2	41.1	75.8	91.3	14.3	24.1	50.6	43.5	72.2	63
	(α)		0.95	1.49	1.77	3.08	4.23		2.09	2.03	2.96	5.45	6.57		1.69	3.54	3.04	5.05	4.41
		22.5		1.57	1.87	3.25	4.46			0.97	1.41	2.6	3.14			2.1	1.8	3	2.61
					1.19	2.07	2.84				1.46	2.69	3.24				0.86	1.43	1.25
						1.74	2.39					1.84	2.22					1.66	1.45
							1.37						1.2						0.87
1	K_d		14.4	21.6	28.6	45.8	66.6	9.62	21.6	13.9	33.3	63.9	63.9	10.1	15.1	39.7	31.9	61.9	39.9
	(α)		1.08	1.62	2.15	3.44	5.01		2.25	1.44	3.46	6.64	6.64		1.5	3.93	3.16	6.13	3.95
		13.3		1.5	1.99	3.18	4.63			0.64	1.54	2.96	2.96			2.63	2.11	4.1	2.64
					1.32	2.12	3.08				2.4	4.6	4.6				0.8	1.56	1.01
						1.6	2.33					1.92	1.92	.				1.94	1.25
							1.45						1						0.64
2	K_d		6.4	13.6	15.4	21.3	30.2	3.92	11.7	6.46	20.9	44.2	25.8	3.6	6.7	25.3	15.3	50.8	19.3
	(α)		1.16	2.47	2.8	3.87	5.49		2.98	1.65	5.33	11.3	6.58		1.86	7.03	4.25	14.1	5.36
		5.5		2.125	2.41	3.33	4.72			0.55	1.79	3.78	2.21			3.78	2.28	7.58	2.88
					1.13	1.57	2.22				3.24	6.84	3.99				0.6	2.01	0.76
						1.38	1.96					2.11	1.23					3.32	1.26
							1.42						0.58						0.38
4	K_d		1.2	4.1	4.66	4.6	7.4	1.11	4.1	1.11	7.82	23.7	7.14	1.2	1.6	11.6	3.1	31.6	4.6
	(α)		0.92	3.15	3.58	3.53	5.7		3.69	1	7.05	21.4	6.43		1.33	9.67	2.58	26.3	3.83
		1.3		3.41	3.88	3.83	6.16			0.27	1.91	5.78	1.74			7.25	1.94	19.8	2.88
					1.13	1.12	1.8				7.05	21.4	6.43				0.27	2.72	0.4
						0.98	1.59					3.03	0.91					10.2	1.48
							1.6						0.3						0.15

Table 5
K_d values and separation factors (α) for Ni^{2+}, Cd^{2+}, Co^{2+}, Pb^{2+}, Zn^{2+}, and/or Cu^{2+} onto [P(AM-AN)-MgSi] at different radiation dose at 25°C ± 1°C.

$[H^+]$	K_d mL/g and (α)	[P(AM-AN)-MgSi] at dose 25 kGy						[P(AM-AN)-MgSi] at dose 65 kGy						[P(AM-AN)-MgSi] at dose 90 kGy					
		Co^{2+}	Ni^{2+}	Cu^{2+}	Zn^{2+}	Cd^{2+}	Pb^{2+}	Pb^{2+}	Ni^{2+}	Cd^{2+}	Cu^{2+}	Zn^{2+}	Co^{2+}	Cu^{2+}	Zn^{2+}	Co^{2+}	Pb^{2+}	Ni^{2+}	Cd^{2+}
10^{-3}	K_d	57	166	208	216	380	760	64.3	124	154	155	224	260	58.8	86.3	87	88.7	189	189
	(α)		2.91	3.65	3.79	6.67	13.3		1.93	2.4	2.41	3.48	4.04		1.48	1.48	1.51	3.21	3.21
				1.25	1.3	2.29	4.58			1.24	1.25	1.81	2.1			1.01	1.03	2.19	2.19
					1.04	1.83	3.65				1.01	1.45	1.69				1.02	2.17	2.17
						1.76	3.52					1.45	1.68					2.13	2.13
							2						1.16						1
10^{-2}	K_d	55.9	125	204	214	350	697	62.3	109	145	154	218	255	56.9	86.4	82.7	87.2	183	182
	(α)		2.24	3.65	3.83	6.26	12.5		1.75	2.33	2.47	3.5	4.09		1.52	1.45	1.53	3.22	3.2
				1.63	1.71	2.8	5.58			1.33	1.41	2	2.34			0.96	1.01	2.12	2.11
					1.05	1.72	3.42				1.06	1.5	1.76				1.05	2.21	2.2
						1.64	3.26					1.42	1.66					2.1	2.1
							1.99						1.17						0.99
10^{-1}	K_d	54.8	92	199	200	274	658	59.4	94.4	140	140	195	235	55.6	83.2	79	84.1	168	170
	(α)		1.68	3.63	3.65	5	12		1.59	2.36	2.36	3.28	3.97		1.5	1.42	1.51	3.02	3.06
				2.16	2.17	2.98	7.15			1.48	1.48	2.07	2.49			0.95	1.01	2.02	2.04
					1.01	1.38	3.31				1	1.39	1.68				1.06	2.13	2.15
						1.37	3.29					1.39	1.68					2	2.02
							2.4						1.2						1.01
0.5	K_d	50.6	32.2	105	79.9	166	226	27.2	69.1	98.9	75	109	164	46.5	49.2	48.8	53.7	134	141
	(α)		0.64	2.08	1.58	3.28	4.47		2.54	3.64	2.76	4.01	6.03		1.06	1.05	1.15	2.88	3.03
				3.26	2.48	5.16	7.02			1.43	1.09	1.58	2.37			0.99	1.09	2.72	2.87
					0.76	1.58	2.15				0.76	1.1	1.66				1.1	2.75	2.89
						2.08	2.83					1.45	2.19					2.5	2.63
							1.36						1.5						1.05
1	K_d	30.4	15.9	46.3	49.6	57.6	85.1	20.3	26.5	73.6	41.4	63.9	63.1	25.5	22.5	26.3	28.6	80.2	78.7
	(α)		0.52	1.52	1.63	1.89	2.8		1.31	3.63	2.04	3.15	3.11		0.88	1.03	1.12	3.15	3.09
				2.91	3.12	3.62	5.35			2.78	1.56	2.41	2.38			1.17	1.27	3.56	3.5
					1.07	1.24	1.84				0.56	0.87	0.86				1.09	3.05	2.99
						1.16	1.72					1.54	1.52					2.8	2.75
							1.48						0.99						0.98
2	K_d	13.8	2.95	15.4	10.7	12.2	19.1	6.79	11	28.7	18.9	26	20.2	12.2	5.44	11.7	15.7	63.3	39.1
	(α)		0.21	1.12	0.78	0.88	1.38		1.62	4.23	2.78	3.83	2.97		0.45	0.96	1.29	5.19	3.2
				5.22	3.63	4.14	6.47			2.61	1.72	2.36	1.84			2.15	2.89	11.6	7.19
					0.69	0.79	1.24				0.66	0.91	0.7				1.34	5.41	3.34
						1.14	1.79					1.38	1.07					4.03	2.49
							1.57						0.78						0.62
4	K_d	4.05	0.09	0.43	0.72	2.1	1.55	0.94	1.72	9.25	1.51	3.5	1.94	2.02	0.55	1.06	3.98	11.3	16.2
	(α)		0.02	0.11	0.18	0.52	0.38		1.83	9.84	1.61	3.72	2.06		0.27	0.52	1.97	5.59	8.02
				4.78	8	23.3	17.2			5.38	0.88	2.03	1.13			1.93	7.2	20.5	29.5
					1.67	4.89	3.6				0.16	0.38	0.21				3.75	10.7	15.3
						2.92	2.15					2.32	1.28					2.84	4.07
							0.74						0.55						1.43

65 kGy. And Cd^{2+} has a higher separation factor by (4.5, 2.8, 1.8, 1.7, and 1.3) for Pb^{2+}, Zn^{2+}, Co^{2+}, Cu^{2+}, and Ni^{2+}, respectively, at 90 kGy. These values indicated that Cd^{2+} can easily separate from radioactive and industrial waste solutions included the above-mentioned cations [17], and reveal that non-selectivity of P(AM-AN) for Zn^{2+}.

Figs. 3e–g and Table 5 show that the $[H^+]$ dependency of K_d values of studied cations onto [P(AM-AN)-MgSi] at different radiation doses. Linear relations between $\log K_d$ and $[H^+]$ were observed for Ni^{2+}, Cd^{2+}, Co^{2+}, Pb^{2+}, Zn^{2+}, and Cu^{2+} with slopes [(0.78, 0.58, 0.29, 0.68, 0.62, and 0.66)], [(0.46, 0.31, 0.54, 0.46, 0.45, and 0.49)], and [(0.31, 0.27, 0.47, 0.34, 0.56, and 0.37)] for [P(AM-AN)-MgSi] at 25, 65, and 90 kGy, respectively. These slopes are smaller than the valence of the metal ions sorbed, which proves the non-ideality of the exchange reaction. The variation may be due to the prominence of different mechanisms other than ion-exchange reactions [26].

Table 5 indicates that the K_d have the sequence order of studied cations absorbed on [P(AM-AN)-MgSi] at 25 kGy is $Pb^{2+} > Cd^{2+} > Zn^{2+} \geq Cu^{2+} > Ni^{2+} > Co^{2+}$ while the selectivity order at 65 kGy is $Co^{2+} > Zn^{2+} > Cu^{2+} \approx Cd^{2+} > Ni^{2+} > Pb^{2+}$ and the selectivity order at 90 kGy is $Cd^{2+} \approx Ni^{2+} > Pb^{2+} \approx Co^{2+} \approx Zn^{2+} > Cu^{2+}$. This sequence order supports the sorption of metal ions as hydrated state for [P(AM-AN)-MgSi] at 25 and 90 kGy except Ni^{2+} adsorbed as unhydrated state at 90 kGy, while the sorption of metal ions as unhydrated state for [P(AM-AN)-MgSi] at 65 kGy, which may be due to the ionic radii [35–37] The separation factors for the studied cations on [P(AM-AN)-MgSi] were calculated and indicated that, Pb^{2+} has a higher separation factor by (13.3, 4.6, 3.7, 3.5, and 2) for Co^{2+}, Ni^{2+}, Cu^{2+}, Zn^{2+}, and Cd^{2+}, respectively, at 25 kGy. While Co^{2+} has a higher separation factor by (4.0, 2.1, 1.7, 1.68, and 1.16) for Pb^{2+}, Ni^{2+}, Cd^{2+}, Cu^{2+}, and Zn^{2+}, respectively, at 65 kGy. And Cd^{2+} has a higher separation factor by (3.2, 2.19, 2.17, 2.13, and 1) for Cu^{2+}, Zn^{2+}, Co^{2+}, Pb^{2+}, and Ni^{2+}, respectively, at 90 kGy. These values indicated that Pb^{2+}, Co^{2+}, Cd^{2+} can easily separate from radioactive and industrial waste solutions included the above-mentioned cations at 25, 65, and 90 kGy, respectively [11,34].

References

[1] M.P. Aji, P.A. Wiguna, J. Karunawan, A.L. Wati, Removal of heavy metal nickel-ions from wastewaters using carbon nanodots from frying oil, Procedia Eng., 170 (2017) 36–40.

[2] H. Leinonen, J. Lehto, Ion-exchange of nickel by iminodiacetic acid chelating resin Chelex 100, React. Funct. Polym., 43 (2000) 1–6.

[3] X. Liu, R. Ma, X. Wang, Y. Ma, Y. Yang, L. Zhuang, S. Zhang, R. Jehan, J. Chen, X. Wang, Graphene oxide-based materials for efficient removal of heavy metal ions from aqueous solution: a review, Environ. Pollut., 252 (2019) 62–73.

[4] S.H. Lin, S.L. Lai, H.G. Leu, Removal of heavy metals from aqueous solution by chelating resin in a multistage adsorption process, J. Hazard. Mater., 76 (2000) 139–153.

[5] G. Sharma, M. Naushad, D. Pathania, A. Kumar, A multifunctional nanocomposite pectin thorium(IV) tungstomolybdate for heavy metal separation and photoremediation of malachite green, Desal. Water Treat., 57 (2016) 19443–19455.

[6] G. Sharma, M. Naushad, A.H. Al-Muhtaseb, A. Kumar, M.R. Khan, S. Kalia, Shweta, M. Bala, A. Sharma, Fabrication and characterization of chitosan-crosslinked-poly(alginic acid) nanohydrogel for adsorptive removal of Cr(VI) metal ion from aqueous medium, Int. J. Biol. Macromol., 95 (2017) 484–493.

[7] G. Sharma, A. Kumar, M. Naushad, A. Kumar, A.H. Al-Muhtaseb, P. Dhiman, A.A. Ghfar, F.J. Stadler, M.R. Khan, Photoremediation of toxic dye from aqueous environment using monometallic and bimetallic quantum dots based nanocomposites, J. Cleaner Prod., 172 (2016) 2919–2930.

[8] G. Sharma, V.K. Gupta, S. Agarwal, S. Bhogal, M. Naushad, A. Kumar, F.J. Stadler, Fabrication and characterization of trimetallic nano-photocatalyst for remediation of ampicillin antibiotic, J. Mol. Liq., 260 (2018) 342–350.

[9] D. Pathania, G. Sharma, M. Naushad, V. Priya, A biopolymer-based hybrid cation exchanger pectin cerium(IV) iodate: synthesis, characterization, and analytical applications, Desal. Water Treat., 57 (2016) 468–475.

[10] M.M. Abou-Mesalam, M.R. Abass, M.A. Abdel-Wahab, E.S. Zakaria, A.M. Hassan, H.F. Khalil, Complex doping of d-block elements cobalt, nickel and cadmium in magneso-silicate composite and its use in the treatment of aqueous waste, Desal. Water Treat., 57 (2016) 25757–25764.

[11] E.A. Abdel-Galil, A.B. Ibrahim, M.M. Abou-Mesalam, Sorption behavior of some lanthanides on polyacrylamide stannic molybdophosphate as organic–inorganic composite, Int. J. Ind. Chem., 7 (2016) 231–240.

[12] A.A. Khan, M.M. Alam, Preparation, characterization and analytical applications of a new and novel electrically conducting fibrous type polymeric–inorganic composite material: polypyrrole Th(IV) phosphate used as a cation-exchanger and Pb(II) ion-selective membrane electrode, Mater. Res. Bull., 40 (2005) 289–305.

[13] H. Pang, Y. Wu, X. Wang, B. Hu, X. Wang, Recent advances in composites of graphene and layered double hydroxides for water remediation: a review, Chem. Asian J., 14 (2019) 2542–2552.

[14] Inamuddin, M. Luqman, Ion Exchange Technology I: Theory and Materials, Springer Science & Business Media, Netherlands, 2012.

[15] M.M. Abou-Mesalam, I.M. El-Naggar, Selectivity modification by ion memory of magneso-silicate and magnesium alumino-silicate as inorganic sorbents, J. Hazard. Mater., 154 (2008) 168–174.

[16] Inamuddin, M. Luqman, Ion Exchange Technology II: Applications, Springer Science & Business Media, Netherlands, 2012.

[17] I.M. El-Naggar, M.M. Abou-Mesalam, Novel inorganic ion exchange materials based on silicates; synthesis, structure and analytical applications of magneso-silicate and magnesium alumino-silicate sorbents, J. Hazard. Mater., 149 (2007) 686–692.

[18] I.M. AIi, Y.H. Kotp, I.M. EI-Naggar, Sorption mechanism of some heavy metal ions from aqueous media using magnesium silicate, Arab J. Nucl. Sci. Appl., 43 (2010) 101–113.

[19] I.M. Ali, Y.H. Kotp, I.M. El-Naggar, Thermal stability, structural modifications and ion exchange properties of magnesium silicate, Desalination, 259 (2010) 228–234.

[20] W. Clowutimon, P. Kitchaiya, P. Assawasaengrat, Adsorption of free fatty acid from crude palm oil on magnesium silicate derived from rice husk, Eng. J., 15 (2011) 15–26.

[21] I.M. Ali, E.S. Zakaria, M.M. Ibrahim, I.M. El-Naggar, Synthesis, structure, dehydration transformations and ion exchange characteristics of iron-silicate with various Si and Fe contents as mixed oxides, Polyhedron, 27 (2008) 429–439.

[22] M.M. Abou-Mesalam, A.S. Amin, M.M. Abdel-Aziz, I.M. El-Naggar, Synthesis and ion exchange characteristics of poly (acrylamide-acrylic acid)-silicon titanate and its use for the treatment of industrial wastes, Egypt. J. Chem., 46 (2003) 655–670.

[23] M.M. Abou-Mesalam, M.R. Abass, M.A. Abdel-Wahab, E.S. Zakaria, A.M. Hassan, Polymeric composite materials based on silicate: II. Sorption and distribution studies of some hazardous metals on irradiated doped polyacrylamide acrylic acid, Desal. Water Treat., 109 (2018) 176–187.

[24] M.M. Abou-Mesalam, Structural and crystallographic features of chemically synthesized cero-and titanium cero-antimonates inorganic ion exchangers and its applications, Adv. Chem. Eng. Sci., 1 (2011) 1–8.

[25] M.M. Abou-Mesalam, Retention behavior of nickel, copper, cadmium and zinc ions from aqueous solutions on silico-titanate and silico-antimonate used as inorganic ion exchange materials, J. Radioanal. Nucl. Chem., 252 (2002) 579–583.
[26] Y.F. El-Aryan, E.A. Abdel-Galil, G.E.S. El-deen, Synthesis, characterization and adsorption behavior of cesium, cobalt, and europium on organic-inorganic hybrid exchanger, Russ. J. Appl. Chem., 88 (2015) 516–523.
[27] A. Nilchi, A. Khanchi, H. Atashi, A. Bagheri, L. Nematollahi, The application and properties of composite sorbents of inorganic ion exchangers and polyacrylonitrile binding matrix, J. Hazard. Mater., 137 (2006) 1271–1276.
[28] M.M. Abou-Mesalam, M.R. Abass, A.B. Ibrahim, E.S. Zakaria, A.M. Hassan, Polymeric composite materials based on silicate; I-Synthesis, characterization and formation mechanism, Int. J. Innovative Res. Growth, 6 (2018) 66–82.
[29] S.A. Nabi, S. Usmani, N. Rahman, Synthesis, characterization and analytical applications of an ion-exchange material: zirconium (IV) iodophosphate, Ann. Chim. Fr., 21 (1996) 521–530.
[30] W. Chen, Z. Lu, B. Xiao, P. Gu, W. Yao, J. Xing, A.M. Asiri, K.A. Alamry, X. Wang, S. Wang, Enhanced removal of lead ions from aqueous solution by iron oxide nanomaterials with cobalt and nickel doping, J. Cleaner Prod., 211 (2019) 1250–1258.
[31] P. Gu, S. Zhang, C. Zhang, X. Wang, A. Khan, T. Wen, B. Hu, A. Alsaedi, T. Hayat, X. Wang, Two-dimensional MAX-derived titanate nanostructures for efficient removal of Pb(II), Dalton Trans., 48 (2019) 2100–2107.
[32] M. Saifuddin, P. Kumaran, Removal of heavy metal from industrial wastewater using chitosan coated oil palm shell charcoal, Electron. J. Biotechnol., 8 (2005) 43–53.
[33] H. Moloukhia, Use of animal charcoal prepared from the bivalve chaelatura (chaelatura) companyoi in treatment of waste solution containing cesium and strontium ions, J. Radiat. Res. Appl. Sci., 3 (2010) 343–356.
[34] E.A. Abdel-Galil, Chemical Studies and Sorption Behavior of Some Hazardous Metal Ions on Polyacrylamide Stannic(IV) Molybdophosphate as 'Organic–Inorganic' Composite Cation–Exchanger, Ph.D. Thesis, Chemistry Department, Faculty of Science, Ain Shams University, Cairo, Egypt, 2010.
[35] G. Sharma, D. Pathania, M. Naushad, Preparation, characterization, and ion exchange behavior of nanocomposite polyaniline zirconium(IV) selenotungstophosphate for the separation of toxic metal ions, Ionics, 21 (2015) 1045–1055.
[36] I.M. El-Naggar, E.A. Mowafy, E.A. Abdel-Galil, M.F. El-Shahat, Synthesis, characterization and ion-exchange properties of a novel 'organic–inorganic'hybrid cation-exchanger: poly-acrylamide Sn(IV) molybdophosphate, Global J. Phys. Chem., 1 (2010) 91–106.
[37] S.A. Shady, Selectivity of cesium from fission radionuclides using resorcinol–formaldehyde and zirconyl-molybdopyrophosphate as ion-exchangers, J. Hazard. Mater., 167 (2009) 947–952.